Bioconjugate Chemistry

Article

Cite This: Bioconjugate Chem. XXXX, XXX, XXX-XXX

pubs.acs.org/bc

Evaluation of a Centyrin-Based Near-Infrared Probe for Fluorescence-Guided Surgery of Epidermal Growth Factor Receptor Positive Tumors

Sakkarapalayam M. Mahalingam,[†,‡] Vadim Y. Dudkin,[§] Shalom Goldberg,[§] Donna Klein,[§] Fang Yi,[§] Sunil Singhal,[∥] Karyn T. O'Neil,[*,§] and Philip S. Low[*,†,‡]

[†]Department of Chemistry and [‡]Institute for Drug Discovery, Purdue University, West Lafayette, Indiana 47907, United States

[§]Janssen Research & Development, 1400 McKean Road, Springhouse, Pennsylvania 19477, United States

[∥]Department of Surgery, University of Pennsylvania Perelman School of Medicine, Philadelphia, Pennsylvania 19104, United States

Supporting Information

ABSTRACT: Tumor-targeted near-infrared fluorescent dyes have the potential to improve cancer surgery by enabling surgeons to locate and resect more malignant lesions where good visualization tools are required to ensure complete removal of malignant tissue. Although the tumor-targeted fluorescent dyes used in humans to date have been either small organic molecules or high molecular weight antibodies, low molecular weight protein scaffolds have attracted significant attention because they penetrate solid tumors almost as efficiently as small molecules, but can be infinitely mutated to bind almost any antigen. Here we describe the use of a 10 kDa protein scaffold, a Centyrin, to target a near-infrared fluorescent dye to tumors that overexpress the epidermal growth factor receptor (EGFR) for fluorescence-guided surgery (FGS). We have developed and optimized the dose and time required for imaging small tumor burdens with minimal background fluorescence in real-time fluorescence-guided surgery of EGFR-expressing tumor xenografts in murine models. We demonstrate that the Centyrin-near-infrared dye conjugate (CNDC) binds selectively to human EGFR$^+$ cancer cells with an EC_{50} of 2 nM, localizes to EGFR$^+$ tumor xenografts in athymic nude mice and that uptake of the dye in xenografts is significantly reduced when EGFR are blocked by preinjection of excess unlabeled Centyrin. Taken together, these data suggest that CNDCs can be used for intraoperative identification and surgical removal of EGFR-expressing lesions and that Centyrins targeted to other tumor-specific antigens should prove similarly useful in fluorescence guided surgery of cancer. In addition, we demonstrate that the CNDC is detected in the NIR region of the spectrum and can be utilized for fluorescence-guided surgery (FGS). In addition, we propose that with its eventual complete clearance from EGFR-negative tissues and its quantitative retention in the tumor mass for >24 h, a Centyrin-targeted NIR dye should provide excellent tumor contrast when injected at least 6−8 h before initiation of cancer surgery in human patients.

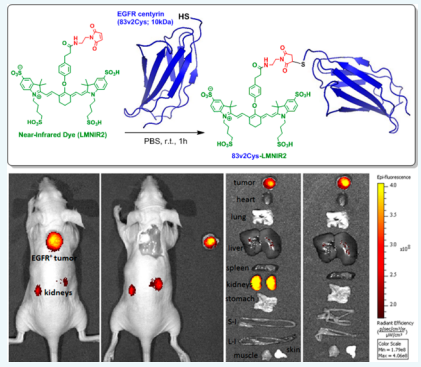

INTRODUCTION

Surgical resection constitutes the primary treatment for most solid tumors, since complete removal of all malignant disease remains the most effective cure for cancer. Although many imaging techniques are available for preoperative diagnosis and staging of cancer, most of these imaging modalities cannot be used intraoperatively because repeated exposure of the surgery staff to the associated ionizing radiation is too dangerous to the surgery staff, the time between data collection and image reconstruction is too long, or the mobility/flexibility of the imaging instrumentation is excessively cumbersome. As a consequence, surgeons must still rely primarily on subtle differences in tissue morphology, coloration, or rigidity to distinguish malignant from healthy tissues. While large tumor masses can be readily identified using these latter techniques, small malignant lesions, boundaries between cancer and healthy tissues, and buried malignant lymph nodes cannot be reliably distinguished by such methodologies.

Fluorescence-guided surgery is an emerging technique that uses either tumor-targeted or tumor-activated fluorescent dyes to illuminate cancerous tissues during surgery, allowing real time intraoperative localization of tumor nodules.[1] Our lab has previously developed fluorescent probes that are targeted to a folate receptor that is overexpressed in ovarian, lung, endometrial, kidney, and other cancers.[2−4] Proof-of-principle studies in patients with ovarian, lung, and kidney cancers have recently demonstrated that folate-conjugated fluorescent dyes can enable resection of significantly more malignant lesions than was possible by other standard techniques.[5−11] Unfortunately, folate receptors are only overexpressed in a subset of human cancers, raising the need for additional tumor-targeting ligands to deliver near-infrared (NIR) fluorescent dyes to folate receptor negative cancers.

Received: September 18, 2017
Published: September 25, 2017

DOI: 10.1021/acs.bioconjchem.7b00566
Bioconjugate Chem. XXXX, XXX, XXX−XXX

The human epidermal growth factor receptor (EGFR) is known to be overexpressed in many types of cancers, including cancers of the head and neck, pancreas, lung, colon, breast, and ovaries, among others.[12,13] Although currently available monoclonal antibodies to EGFR show high affinity and specificity for the aforementioned malignancies, they do not constitute ideal ligands for fluorescence-guided surgery because they clear too slowly from EGFR-negative tissues for use during same-day surgeries[14−16] and often do not yield the tumor contrast of smaller molecular weight targeting ligands.[5−11] While a low molecular weight EGFR-specific organic molecule could conceivably be exploited to deliver a fluorescent dye to EGFR-expressing tumors, no EGFR-specific ligand exists that both binds an externally exposed site on EGFR and does not simultaneously activate the receptor. In order to generate a high affinity EGFR-specific ligand that can be injected shortly before surgery, we searched for a low molecular weight protein scaffold that would exhibit high affinity and specificity for EGFR. In this paper we demonstrate that an EGFR-specific Centyrin, a novel class of protein scaffold molecules developed by O'Neil and co-workers,[17] provides the specificity of an antibody with the size (~10 kDa) and stability of a small organic molecule. Here we report the first application of a Centyrin for *in vivo* tumor imaging by conjugating the EGFR-specific Centyrin to a highly fluorescent near-infrared (NIR) dye.

RESULTS

Affinity Determination of 83v2 Binding to Recombinant Human and Murine EGFR *In Vitro*. Binding affinities of 83v2 to murine or human EGFR were nearly identical with measured intrinsic affinity of 0.6 nM for either receptor. Thus, in a murine xenograft model, 83v2 is expected to bind both normal murine EGFR$^+$ tissues and human EGFR$^+$ tumor cells.

	k_{on} (1/Ms)	k_{off} (1/s)	KD (nM)
Human EGFR-Fc	5.30×10^{04}	2.90×10^{-05}	0.55
Murine EGFR-Fc	4.99×10^{04}	3.13×10^{-05}	0.63

Synthesis and Characterization of Centyrin NIR Dye Conjugate (CNDC). The low molecular weight Centyrin (83v2Cys) modified with a single cysteine for conjugation was selected as the targeting ligand for delivery of the near-infrared (NIR) dye (S0456) to EGFR positive tumors. As shown in Scheme 1, 83v2Cys was coupled to LMNIR2 in PBS buffer using maleimide chemistry. The final Centyrin-NIR dye conjugate was obtained in a total overall yield of 42%, purified by PD10 size exclusion column chromatography, and named CNDC. The total molecular weight of the conjugate is 12 814 Da and its fluorescence excitation and emission maxima are λ_{ex} = 770 nm, λ_{em} = 790 nm.

Analysis of CNDC Binding to HCC827 Cells *In Vitro*. EGFR-positive HCC827 cells were used to evaluate EGFR-mediated binding and endocytosis of CNDC. As seen in Figure 1, following incubation of HCC827 cells with 100 nM CNDC for 1 h at 37 °C, fluorescence is seen both on the surfaces and within the interiors of the cultured HCC827 cells. Moreover, upon coincubation of the same cells with CNDC in the presence of excess Centyrin (83v2Cys), all cell surface and internal fluorescence is eliminated, suggesting that binding and

Scheme 1. Synthesis of the Centyrin Near-Infrared Dye Labeling Reagent[a]

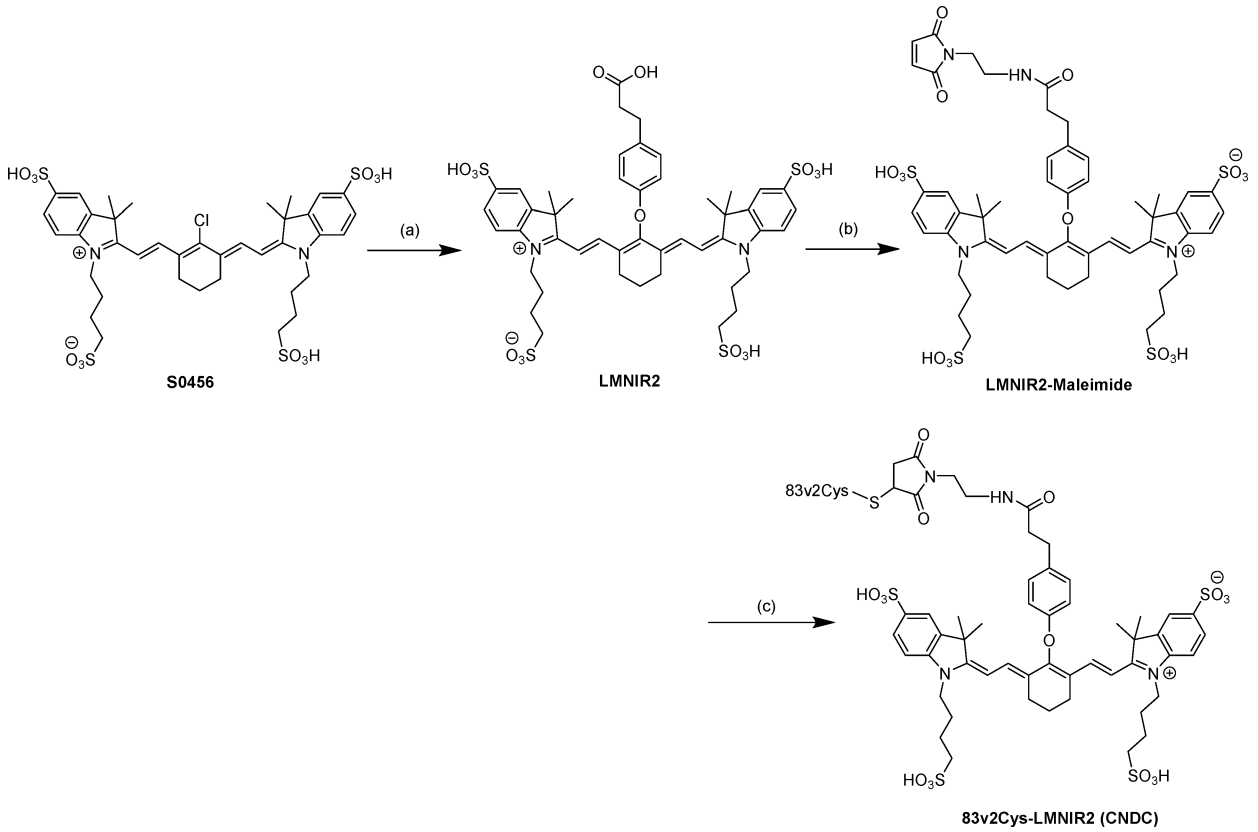

[a]Reagents and conditions: (a) 3-(4-Hydroxyphenyl)-propionic acid, KOH (2 equiv), DMSO, 60 °C, 60 min; (b) (i) HATU, DIPEA, DMSO, r.t. 25 min; (ii) *N*-(2-aminoethyl)-malemide trifluoroacetate salt (2 equiv) stir overnight; (iii) isopropanol, centrifugation; (c) 83v2Cys in PBS and gentle mixing for 60 min.

DOI: 10.1021/acs.bioconjchem.7b00566
Bioconjugate Chem. XXXX, XXX, XXX−XXX

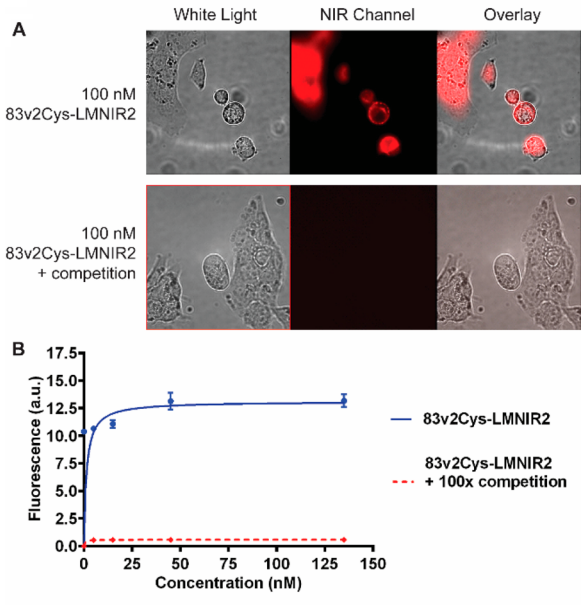

Figure 1. Binding of the Centyrin near-infrared dye conjugate (CNDC) to HCC827 cells. (A) HCC827 cells were incubated with 100 nM CNDC in the presence or absence to 100-fold excess of unlabeled Centyrin (83v2Cys). (B) HCC827 cells were incubated with increasing concentrations of CNDC in the presence or absence to 100-fold excess of unlabeled Centyrin, 83v2Cys. Data are mean ± SEM of $n = 3$.

uptake of the fluorescence seen in the absence of excess competing ligand is EGFR-mediated.

Quantitative analysis of EGFR-specific binding was conducted by measuring cell-associated fluorescence following incubation of the HCC827 cells with increasing concentrations of CNDC. As shown in Figure 1B, binding was found to be saturable with an apparent dissociation constant of 1.4 nM (blue curve). Binding was also quantitatively inhibited when a 100-fold molar excess of unconjugated Centyrin was coincubated with the CNDC (red curve).

***In Vivo* Imaging and Biodistribution.** In order to determine whether CNDC can specifically label EGFR-expressing tumors *in vivo*, mice with HCC827 xenografts were injected via the tail vein with 10 nmol CNDC and imaged over the subsequent 48 h period. As shown in Figure 2, tumor accumulation of CNDC began at 4 h and reached its peak fluorescence between 6 and 12 h.

To further ensure that the fluorescent signal from the tumor was adequate for surgical applications, we next performed a model tumor resection surgery guided by the images obtained with CNDC. One such sequence of surgical procedures is shown Figure 3. In this sequence, the tumor was initially located in the intact animal by NIR fluorescence whole body imaging (panel 1). Next, guided by this image, an incision was made directly over the fluorescent locus to expose the tumor mass (panel 2). With continued aid of the NIR fluorescence image, the cancer tissue was carefully resected and placed to the right of the tumor-bearing mouse for further imaging (panel 3). Finally, to ensure that all malignant disease had been successfully removed, the sensitivity of the camera was increased and the animal was reimaged. As shown in panel 4, this subsequent image revealed the presence of a small pocket of residual cancer, which was then completely resected with the aid of the fluorescence image (tumor-free image not shown).

Live imaging indicated that stably retained fluorescence was primarily confined to the tumor and kidneys, and this was

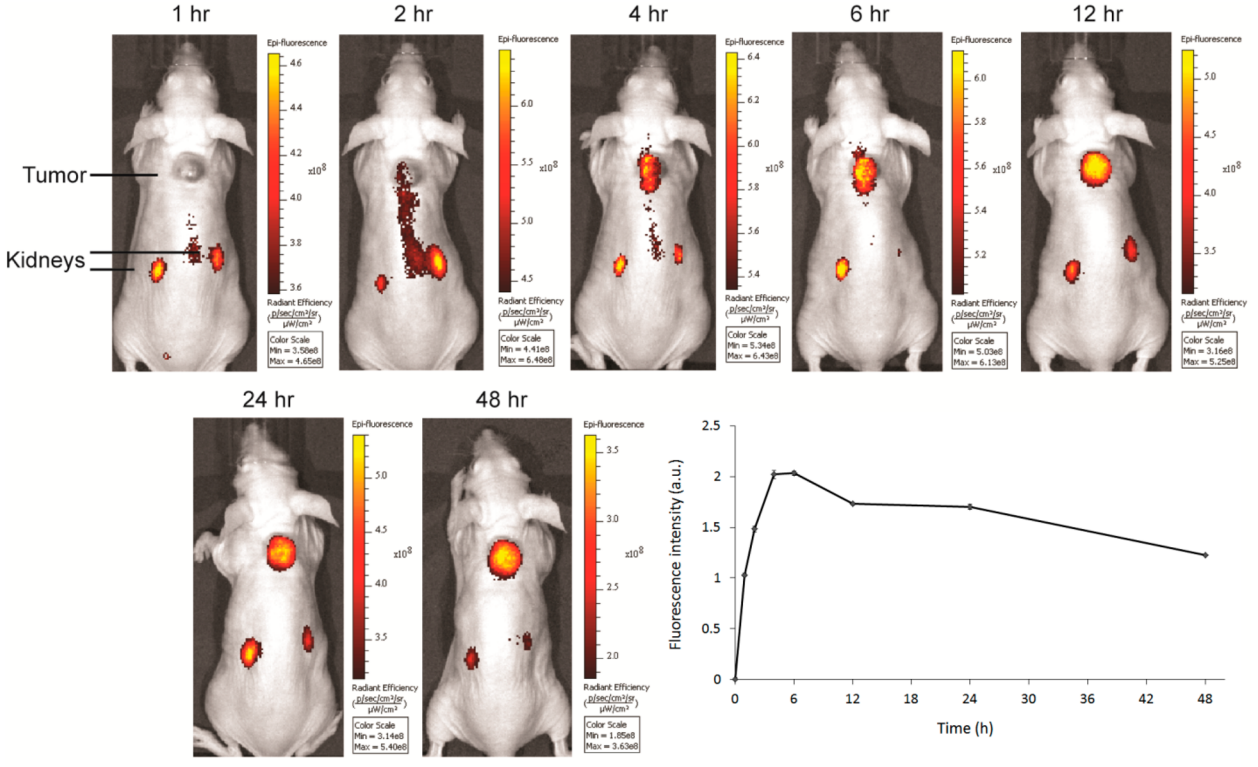

Figure 2. Representative images of HCC827 tumor bearing mice treated with 10 nmol CNDC. Mice were injected via tail vein with 10 nmol CNDC and fluorescence images were acquired over a 48 h period. The graph shows mean fluorescence intensity ± SD for tumors from 3 mice.

DOI: 10.1021/acs.bioconjchem.7b00566
Bioconjugate Chem. XXXX, XXX, XXX−XXX

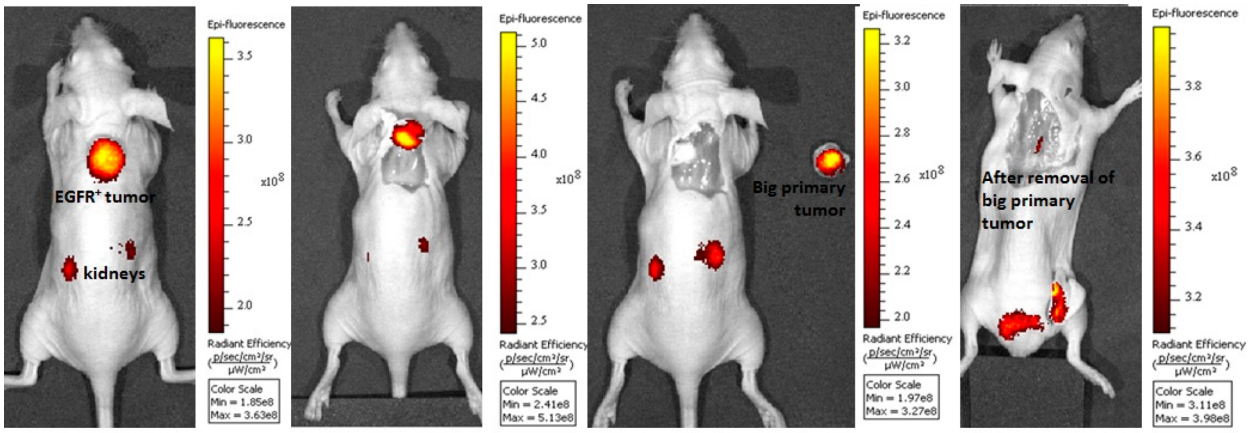

Figure 3. Fluorescence guided surgery of HCC827 tumor bearing mice treated with 10 nmol CNDC injected via tail vein. Fluorescence images were acquired after 48 h and resection of the cancer tissue by fluorescence guided sequence of surgical procedures. Ideal location for making an incision (panel 1); performed the incision and exposed the fluorescent mass (panel 2); resected the cancer tissue and placed the resected mass to the right of the tumor-bearing mouse (panel 3); and subsequent higher sensitivity image revealed the presence of a small pocket of residual cancer (panel 4).

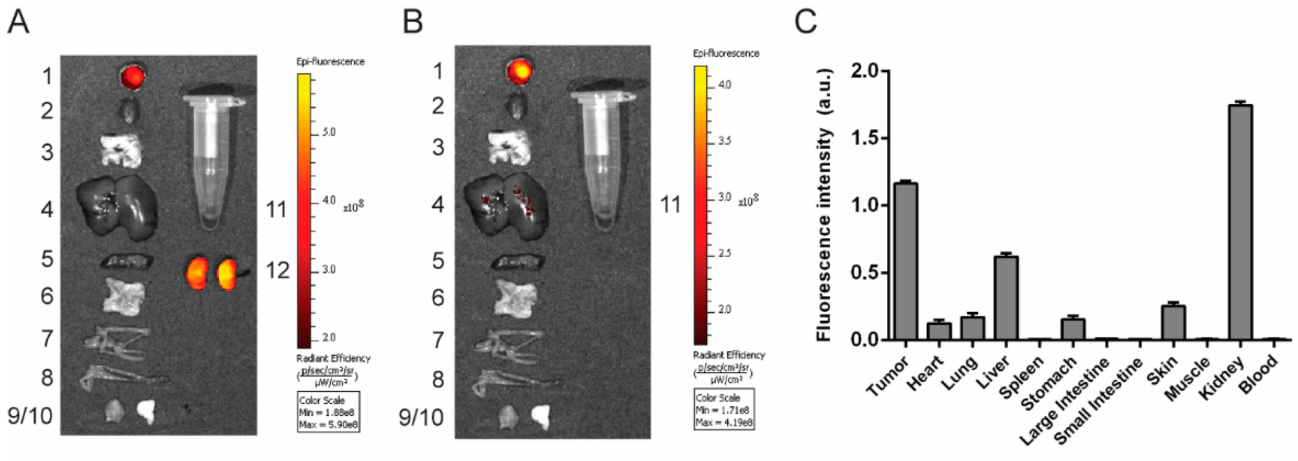

Figure 4. Evaluation of CNDC (10 nmol) accumulation in the internal tissues and organs of the HCC827 tumor bearing mice. Organs and tissues were dissected at 48 h, and panels show (A) all organs and (B) organs excluding kidneys. Organs are labeled as follows: (1) tumor, (2) heart, (3) lungs, (4) liver, (5) spleen, (6) stomach, (7) small intestine, (8) large intestine, (9) muscle, (10) skin, (11) blood, (12) kidneys. (C) Quantification of tissue fluorescence intensity. Data are mean ± SD for 3 mice.

further confirmed when the major organs were excised at 48 h and imaged (Figure 4). The elevated fluorescence in the kidneys and liver (Figure S4) may arise from the known expression of EGFR in these two organs[58,59] and the fact that both kidneys and liver constitute routes of CNDC excretion.

Based on the high affinity binding constant of 1.4 nM observed *in vitro*, we next explored whether lower doses of CNDC might also afford better images of solid tumors *in vivo*. For this purpose, tumor-bearing mice were injected via tail vein with either 5 or 1 nmol CNDC/mouse, and images were again collected as a function of time post-injection. As shown in Figures S5 and S6, similar tumor selectivity was seen at 5 nmol/mouse, while the background CNDC fluorescence cleared much faster at 1 nmol/mouse than at higher CNDC concentrations, allowing distinct visualization of the tumor by 1 h post-injection. More importantly, analogous tumor-to-background ratios were also observed at 1 nmol/mouse, with good tumor resolution again obtained at the 1−2 h time point (Figure 5). Because uptake of fluorescence in the tumor was almost quantitatively blocked by coadministration of 100-fold excess unlabeled Centyrin, we conclude that tumor uptake of CNDC is EGFR-mediated. Moreover, since the majority of fluorescence accumulation in the kidneys could be similarly competed with excess unlabeled Centyrin, we also conclude that much of CNDC retention in the kidneys is EGFR-mediated. The fact that the majority of tumor-specific fluorescence is retained in the tumor mass for at least 24 h further suggests that the lower 1 nmol/mouse dose is probably adequate for most applications in fluorescence-guided surgery.

To obtain an initial indication of the optimal time interval between CNDC injection and image acquisition, the pharmacokinetics of CNDC in live mice was examined. As shown in Figure 6, analysis of the rise and fall of CNDC fluorescence in the blood following intravenous injection revealed that peak fluorescence was seen almost immediately and that clearance from the bloodstream proceeded with a half-life of ∼4 h resulting in nearly complete elimination by the ∼48 h time point. Not surprisingly, lower initial doses of CNDC yielded better tumor:background ratios at longer time points for most organs (Figure 7), again suggesting that the ideal dose of CNDC for fluorescence-guided surgery might lie at the lower end of those examined here.

DOI: 10.1021/acs.bioconjchem.7b00566
Bioconjugate Chem. XXXX, XXX, XXX−XXX

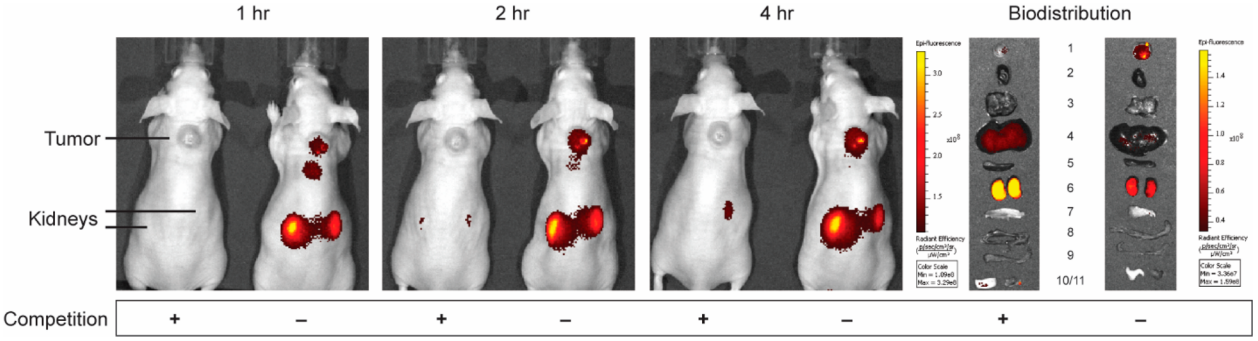

Figure 5. Representative images of HCC827 tumor-bearing mice treated with 1 nmol CNDC in the presence or absence of competing unlabeled Centyrin. Mice were injected via tail vein with 1 nmol CNDC in the presence or absence of a 100-fold excess of 83v2Cys to block all vacant receptor binding sites and fluorescence images were acquired over the ensuing 4 h. Organs and tissues were resected after whole animal imaging at 4 h and are labeled as follows: (1) tumor, (2) heart, (3) lungs, (4) liver, (5) spleen, (6) kidneys, (7) stomach, (8) small intestine, (9) large intestine, (10) skin, (11) muscle.

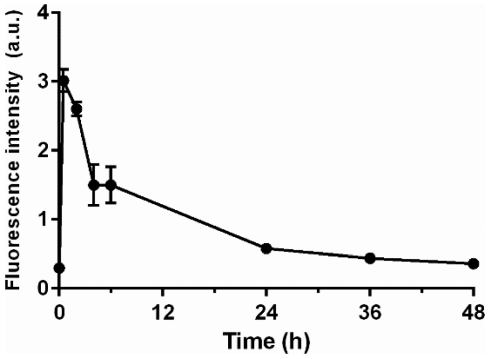

Figure 6. Blood half-life of CNDC in vivo. 10 nmol CNDC was administered intravenously and blood samples were collected over 48 h. The graph shows mean fluorescence intensity ± SD for 3 mice.

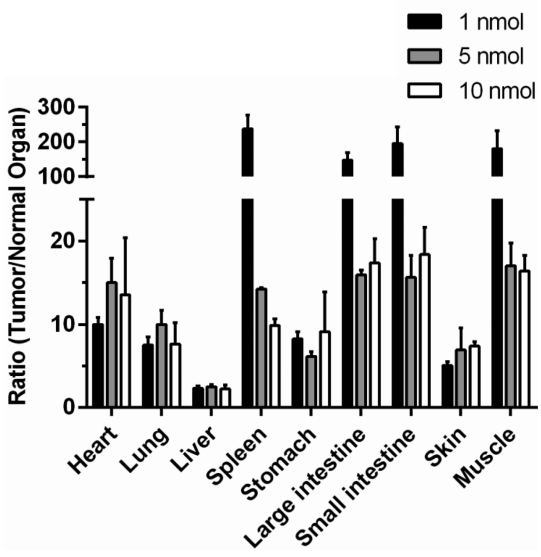

Figure 7. Ratio of fluorescence intensity in tumor/normal organs in HCC827 tumor bearing mice dosed with 1 (100 μL of 10 μM), 5 (100 μL of 50 μM), or 10 (100 μL of 100 μM) nmol of CNDC. Mice were injected via tail vein with the indicated concentrations of CNDC and fluorescence images acquired 4 h (1 nmol), 24 h (5 nmol), and 48 h (10 nmol) post-injection. Data are mean ± SD of $n = 3$.

DISCUSSION

As discussed above, initial clinical trials aimed at examining the use of tumor-targeted fluorescent dyes for identification and resection of malignant lesions during cancer surgery have yielded promising results.[5−9] Buoyed by these data, an increase in research aimed at developing additional tumor-targeted fluorescent dyes has ensued, yielding a dramatic expansion of the tools for fluorescence guided surgery.[11,18−46] Not surprisingly, most new fluorescence imaging agents have relied on either activation of a quenched fluorescent dye by a tumor-specific enzyme[23−38] or binding of a ligand-conjugated dye by a tumor-specific receptor.[39−46] While several of the latter class of dyes have been developed for imaging cancers that overexpress a folate receptor,[5−11] neurokinin 1 receptor,[39] cholecystokinin 2 receptor,[40] prostate-specific membrane antigen receptor,[41−43] CXCR4 receptor,[44] carbonic anhydrase IX,[45,46] and so forth,[47−56] other very tumor-specific proteins have not been targetable with small organic ligands, largely because they are either topographically too featureless, conformationally too flexible, or chemically too unreactive to bind small molecules with high affinity. Thus, to establish high affinity associations with such unreactive surfaces, larger ligands that can establish multiple weak interactions over large surface areas are thought to be essential; and while antibodies constitute the most readily recognized examples of such ligands, their large size has led to undesirable pharmacokinetic properties that significantly limit their use in intraoperative imaging.

In an attempt to identify a ligand as adaptable as an antibody but of considerably smaller size, we looked for a low molecular weight protein scaffold of human origin (i.e., for low immunogenicity) with a stable 3-dimensional structure, good water solubility, low toxicity, single site for dye derivatization, and freely mutatable surface that could be genetically engineered to bind almost any cell surface protein. The Centyrin family of protein scaffolds met all of these requirements and the pre-existing Centyrin that was developed to recognize EGFR (83v2Cys[57]) constituted an ideal test system to assess the feasibility of using a protein scaffold for fluorescence-guided surgery. In this paper we have demonstrated that the Centyrin-NIR dye conjugate directed to EGFR yields very a good tumor:background ratio in minimal time following its intravenous injection. Except for its retention in the kidneys and liver (due to expression of EGFR in these organs)[58,59] and its slow clearance through the liver, the conjugate shows little accumulation in any healthy organs. Thus, for EGFR-positive cancers that neither reside nor metastasize to the kidneys or liver (e.g., cancers of the breast, bladder, colon, etc.),[60] CNDC should constitute a viable candidate for use in fluorescence-guided surgery.

DOI: 10.1021/acs.bioconjchem.7b00566
Bioconjugate Chem. XXXX, XXX, XXX−XXX

The fact that CNDC binds to human and murine EGFR with similar affinity further suggests that the healthy tissue distribution observed in this study should be representative of the healthy tissue uptake in humans.

Although insufficient data exist to draw any firm conclusions, it might still be useful to begin to compare the properties of the first three major classes of ligand-conjugated fluorescent dyes that have been studied *in vivo* to date, namely: (i) low molecular weight organic ligands (e.g., folic acid, $M_R \sim 441$), (ii) protein scaffolds (e.g., an EGFR-binding Centyrin, $M_R \sim 12{,}814$), and (iii) antibodies (e.g., an anti-EGFR antibody, $M_R \sim 150{,}000$). From the limited published reports available to date, it would appear that the affinities of all three ligands for their tumor targets are somewhat similar, i.e., $K_D \sim 10^{-9}$ M.[61,62] Moreover, all three ligand types display some kidney and liver retention, likely due to a combination of receptor expression in those tissue and excretion mechanisms. While the immunogenicity potential of Centyrins has not yet been tested in humans, good stability, solubility, and homogeneity properties have been reported.[57] Nevertheless, several features distinguish Centyrins and antibodies from small molecule ligands. First, the binding regions of antibodies and Centyrins can be almost infinitely mutated to enable binding to most tumor-specific antigens (i.e., including receptors for which low molecular weight ligands are currently unavailable), whereas totally unique low molecular weight ligands must be designed for each different tumor-specific receptor.[39−46] Second, while the half-time for clearance of the anti-EGFR antibody appears to be several days in humans,[13,14] i.e., similar to the half-time for clearance of an anti-EGFR-drug conjugate in man,[15] the half-time for clearance of the EGFR-targeted Centyrin was found to be ∼4 h in mice (and will be somewhat longer in humans) and the half-times for clearance of both folate-fluorescein and folate-NIR dye conjugates in man are ∼30 min. Based on established clinical data, the folate conjugates can be injected immediately prior to cancer surgery, with good contrast emerging within 1−2 h of injection[5−11] while the antibody−dye conjugates must be administered several days prior to surgery to obtain good tumor contrast.[11] Given the more than 8-fold slower clearance of the Centyrin conjugate than folate conjugate in mice, it remains uncertain whether our CNDC might be injected on the same day as surgery in man. However, with its eventual complete clearance from EGFR-negative tissues and its quantitative retention in the tumor mass for >24 h, a Centyrin-targeted NIR dye should provide excellent tumor contrast when injected at least 6−8 h before initiation of cancer surgery in man.

EXPERIMENTAL PROCEDURES

Chemicals. 2-(1*H*-7-Azabenzotriazol-1-yl)-1,1,3,3-tetramethyl uronium hexafluorophosphate methanaminium (HATU) was obtained from Genscript Inc. (Piscataway, New Jersey). 3-(4-Hydroxyphenyl)-propionic acid, diisopropylethylamine (DIPEA), piperidine, dimethyl sulfoxide (DMSO), isopropanol, and all other reagents were purchased from Sigma-Aldrich. For the synthesis of LMNIR2-maleimide, 3-(4-hydroxyphenyl)-propionic acid and *N*-(2-aminoethyl)-maleimide trifluoroacetate salt were purchased from Sigma-Aldrich and S0456 was obtained from Few Chemicals. The Centyrin 83v2Cys was provided by Janssen R&D. Murine EGFR-Fc was purchased from R&D Systems and human EGFR-Fc was prepared by Janssen R&D.

Synthesis of LMNIR2 and LMNIR2-Maleimide. The synthesis of both LMNIR2 and its maleimide conjugate (LMNIR2-Maleimide) was performed as shown in Scheme 1. The chloro near-infrared dye (S0456) was reacted with 3-(4-hydroxyphenyl)-propionic acid in the presence of 2 equiv of KOH, in dimethyl sulfoxide (DMSO) at 60 °C for 60 min to give compound LMNIR2 (near IR dye). The crude product was purified by preparative reverse-phase high-performance liquid chromatography (yield of 68% and final purity of 96%) with a gradient mobile phase consisting of 20 mM ammonium acetate buffer and 5% to 80% acetonitrile over 30 min (xTerra C18; Waters; 10 μm; 19 × 250 mm). Elution of the near IR dye, LMNIR2, was monitored at 280 nm, and the identities of eluted compounds were analyzed by liquid chromatography−mass spectrometry (see Figure S2 Supporting Information).

For synthesis of the maleimide conjugate of LMNIR2, LMNIR2 (1 equiv) dissolved in anhydrous DMSO containing diisopropylethylamine (5 equiv) and HATU (1 equiv) was stirred for 25 min under argon atmosphere. A 3-fold molar excess of *N*-(2-aminoethyl)-maleimide trifluoroacetate salt was then added and stirred overnight at room temperature, as outlined in Scheme 1. The product was precipitated by addition of isopropanol and collected by centrifugation prior to redissolution in DMSO. The crude product was purified by preparative reverse phase HPLC using a mobile phase of A = 20 mM ammonium acetate buffer, pH 7; B = acetonitrile; gradient 0−50% B in 30 min, 13 mL/min, λ = 280 nm. Pure fractions were analyzed by LC-MS and (see Figure S3 in Supporting Information), pooled, and lyophilized to furnish LMNIR2-Maleimide.

Synthesis of Centyrin NIR Dye Conjugate (CNDC). The EGFR-specific Centyrin, 83v2Cys, was obtained by screening a Centyrin library[17] for Centyrins that exhibited high affinity for EGFR and then the selected Centyrin (100−200 μM) was treated with 10 mM TCEP (a reducing agent) and incubated for 30−45 min at room temperature.[58] Excess TCEP was removed by incubation with 3 vol of ammonium sulfate (∼4 M) on ice for 20 min followed by centrifugation at 25 000 rpm for 20 min at 10 °C. After discarding the supernatant the 83v2Cys Centyrin was dissolved in aqueous buffer and same procedure was repeated to remove all traces of TCEP. The reduced Centyrin was then resuspended in ∼3 volumes of ammonium sulfate:PBS mixture (3:1) and again incubated on ice. After centrifugation as above, the supernatant was again discarded and the final pellet was resuspended in PBS. The concentration of protein was then measured using a UV−vis spectrophotometer assuming an extinction coefficient of 83v2Cys is 19 180 mol^{-1} cm^{-1}. For conjugation of the Centyrin to LMNIR2-maleimide, 1.1 equiv of the dye was added to the reduced Centyrin in PBS and stirred gently at room temperature for 60 min (Scheme 1). The crude reaction mixture containing CNDC was purified by size-exclusion chromatography in PBS on a PD10 column using gravity flow. The final concentration of the 83v2Cys-LMNIR2 conjugate in PBS was measured by UV−vis spectrophotometer using an extinction coefficient of 83v2Cys of 19 180 mol^{-1} cm^{-1}.

Affinity Determination of 83v2 Binding to Human and Murine EGFR-Fc. Binding affinity of 83v2 to recombinant human and murine EGFR, both with a C terminal human Fc fusion was measured using a ProteOn XPR-36 instrument (BioRad). Goat anti-human Fc IgG (R&D system) was directly immobilized via amine coupling at 5 μg/mL in acetate buffer, pH 5.0 on all 6 ligand channels in horizontal orientation on a GLC Sensor Chip (Bio-Rad, catalog no. 176−5011) with a flow rate of 30 μL/min in PBS containing 0.005% Tween-20.

DOI: 10.1021/acs.bioconjchem.7b00566
Bioconjugate Chem. XXXX, XXX, XXX−XXX

The immobilization densities averaged about 1500 Response Units (RU) with less than 5% variation among different channels. Human EGFR-Fc and murine EGFR-Fc were captured on the anti-Fc IgG surface each at 2 different concentrations 10, 5 μg/mL in vertical ligand orientation, with final captured level ranging 600−800 Rus. Two ligand channels were used as no antigen surface controls. 83v2 starting at 1 μM in 3-fold dilution series of 5 concentrations flew in as analyte to bind to captured EGFRs in the horizontal orientation. A buffer sample was also injected to monitor the dissociation of captured EGFR-Fc and baseline stability. The dissociation phase for all concentrations of the Centryin was monitored at a flow rate of 100 μL/min for 60 min. The binding surface was regenerated for the next interaction cycle using a 18 s pulse of 0.8% phosphoric acid to remove the EGFR-Fc and bound Centyrin. The raw data were processed by subtracting two sets of reference data from the response data: (1) the interspot signals to correct for the nonspecific interactions between the Centyrin and the empty chip surface; (2) the buffer channel signals to correct for baseline drifting due to the dissociation of captured EGFR-Fc ligand surface over time. The processed data at all concentrations for the Centyrin were globally fit to a 1:1 simple Langmuir binding model to extract estimates of the kinetic (k_{on}, k_{off}) and affinity (K_D) constants.

Analysis of 83v2Cys-LMNIR2 Conjugate Binding to HCC827 Cells. The EGFR-positive HCC827 cell line utilized in these studies was purchased from ATCC (Manassas, VA). HCC827 cells were cultured in RPMI medium supplemented with 10% fetal bovine serum and 1% penicillin streptomycin at 37 °C in a humidified 95% air/5% CO_2 atm. For analysis of the intracellular distribution of CNDC, HCC827 cells were seeded into a confocal dish at a density of 1×10^5 cells per well and allowed to grow to confluence. Cells were then incubated for 1 h at 37 °C with 100 nM of 83v2Cys-LMNIR2 in the presence or absence of 100-fold excess 83v2Cys and rinsed three times with 1 mL of cell culture medium to remove unbound 83v2Cys-LMNIR2. 0.5 mL of fresh medium was then added to each well and images were obtained using a Nikon 90i Fluorescence Microscope. The translocation of fluorescent CNDC from the plasma membrane into intracellular organelles was then followed as a function of time.

For analysis of CNDC binding affinity, HCC827 cells were seeded into 24 well plates (BD Purecoat Amine, BD Biosciences) and allowed to grow to confluence over 48−72 h. Spent medium in each well was replaced with 0.5 mL of fresh medium containing 0.5% bovine serum albumin and increasing concentrations of the CNDC conjugate in the presence or absence of 100-fold excess of 83v2Cys were added. After incubation for 1 h at 37 °C, cells were rinsed with incubation solution (2×1.0 mL) to remove unbound fluorescence and the washed cells were dissolved in 0.5 mL of 1% aqueous sodium dodecyl sulfate. Cell associated fluorescence was then determined by measuring emission of the resulting solution upon excitation at 755 nm. All experiments were performed in triplicate. The dissociation constant (K_D) was calculated from a plot of cell bound fluorescence (a.u.) versus the concentration of fluorescent conjugate added using Graphpad Prism software and assuming a noncooperative single site binding equilibrium.

Generation of Subcutaneous Tumor Using HCC827 Cells in Mice. Athymic female nu/nu mice were purchased from Harlan Laboratories (Indianapolis, IN), maintained on normal rodent chow and housed in a sterile environment on a standard 12 h light and dark cycle for the duration of the study. All animal procedures were approved by the Purdue Animal Care and Use Committee in accordance with NIH guidelines.

Six-week-old mice were inoculated subcutaneously on their shoulders using a 25-gauge needle with HCC827 cells (5.0×10^6 cells/mouse) suspended in 200 μL of culture medium. Growth of the tumors was measured in two perpendicular directions every 2 days using a caliper, and the volumes of the tumors were calculated as $0.5 \times L \times W^2$ (L = measurement of longest axis, and W = measurement of axis perpendicular to L in millimeters). Animals were imaged when the tumors reached 300−400 mm^3 volume (~4 weeks). Experiments on live mice involved at least three mice per group.

Fluorescence Imaging and Analysis of Mice. Tumor-bearing mice were treated via tail vein injection with various concentrations of dye conjugate in the presence or absence of a 100-fold excess of 83v2Cys to block all unoccupied EGFR binding sites. Mice were imaged up to 48 h post-injection using a Caliper IVIS Lumina II Imaging station coupled to a ISOON5160 Andor Nikon camera equipped with Living Image Software Version 4.0. The settings were as follows: lamp level, high; excitation, 745 nm; emission, ICG; epi illumination; binning (M) 4; FOV, 12.5; f-stop, 4; acquisition time, 1 s.

Pharmacokinetics of CNDC in Nude Mice. After IV administration of 10 nmol of CNDC, the CNDC concentration in the blood was measured over the subsequent 48 h using a Caliper IVIS Lumina II Imaging station coupled to a ISOON5160 Andor Nikon camera equipped with Living Image Software Version 4.0.

■ ASSOCIATED CONTENT

Supporting Information

The Supporting Information is available free of charge on the ACS Publications website at DOI: 10.1021/acs.bioconjchem.7b00566.

Fluorescence microscopy images; LC-MS and UV−vis characterization; Imaging; Excitation and emission spectra (PDF)

■ AUTHOR INFORMATION

Corresponding Authors

*E-mail: koneil@its.jnj.com.

*E-mail: plow@purdue.edu.

ORCID

Karyn T. O'Neil: 0000-0002-6490-5664

Philip S. Low: 0000-0001-9042-5528

Notes

The authors declare the following competing financial interest(s): This work was supported in part by a grant from On Target Laboratories. Dr. Philip Low is a co-founder and a member of the Board of Directors of On Target Laboratories.

■ ACKNOWLEDGMENTS

This work was supported in part by a grant from NIH R01 CA193556 (Singhal, Low), On Target Laboratories and Janssen R&D.

■ REFERENCES

(1) Nguyen, Q. T., and Tsien, R. Y. (2013) Fluorescence-guided surgery with live molecular navigation–a new cutting edge. *Nat. Rev. Cancer 13*, 653−662.

(2) Wu, M., Gunning, W., and Ratnam, M. (1999) Expression of folate receptor type alpha in relation to cell type, malignancy, and

differentiation in ovary, uterus, and cervix. *Cancer Epidemiol. Biomarkers Prev. 8*, 775−782.
(3) Parker, N., Turk, M. J., Westrick, E., Lewis, J. D., Low, P. S., and Leamon, C. P. (2005) Folate receptor expression in carcinomas and normal tissues determined by a quantitative radioligand binding assay. *Anal. Biochem. 338*, 284−293.
(4) Kalli, K. R., Oberg, A. L., Keeney, G. L., Christianson, T. J., Low, P. S., Knutson, K. L., and Hartmann, L. C. (2008) Folate receptor alpha as a tumor target in epithelial ovarian cancer. *Gynecol. Oncol. 108*, 619−626.
(5) van Dam, G. M., Themelis, G., Crane, L. M., Harlaar, N. J., Pleijhuis, R. G., Kelder, W., Sarantopoulos, A., de Jong, J. S., Arts, H. J., van der Zee, A. G., et al. (2011) Intraoperative tumor-specific fluorescence imaging in ovarian cancer by folate receptor-alpha targeting: first in-human results. *Nat. Med. 17*, 1315−1319.
(6) Hoogstins, C. E. S., Tummers, Q. R. J. G., Gaarenstroom, K. N., de Kroon, C. D., Trimbos, B. M. J., Bosse, T., Smit, V. T. H. B. M., Vuyk, J., van de Velde, C. J. H., Cohen, A. F., et al. (2016) Novel Tumor-Specific Agent for Intraoperative Near-Infrared Fluorescence Imaging: A translational study in healthy volunteers and patients with ovarian cancer. *Clin. Cancer Res. 22*, 2929−2938.
(7) Koenig, S. G., and Kramer, R. (2017) Accessing structurally diverse near-infrared cyanine dyes for folate receptor-targeted cancer cell staining. *Chem. - Eur. J. 23*, 9306−9312.
(8) De Jesus, E., Keating, J. J., Kularatne, S. A., Jiang, J., Judy, R., Predina, J., Nie, S., Low, P. S., and Singhal, S. (2015) Comparison of folate receptor targeted optical contrast agents for intraoperative molecular imaging. *Int. J. Mol. Imaging 2015*, 1.
(9) Shum, C. F., Bahler, C. D., Low, P. S., Ratliff, T. L., Kheyfets, S. V., Natarajan, J. P., Sandusky, G. E., and Sundaram, C. P. (2016) Novel use of folate-targeted intraoperative fluorescence, OTL38, in Robot-Assisted Laparoscopic Partial Nephrectomy: Report of the First Three Cases. *J. Endourol Case Rep 2*, 189−197.
(10) Keating, J. J., Okusanya, O. T., De Jesus, E., Judy, R., Jiang, J., Deshpande, C., Nie, S., Low, P. S., and Singhal, S. (2016) Intraoperative molecular imaging of lung adenocarcinoma can identify residual tumor cells at the surgical margins. *Mol. Imaging Biol. 18*, 209−218.
(11) Kennedy, G. T., Okusanya, O. T., Keating, J. J., Heitjan, D. F., Deshpande, C., Litzky, L., Albelda, S. M., Drebin, J. A., Nie, S., Low, P. S., and Singhal, S. (2015) The optical biopsy: A novel technique for rapid intraoperative diagnosis of primary pulmonary adenocarcinomas. *Ann. Surg. 262*, 602−609.
(12) Sebastian, S., Settleman, J., Reshkin, S. J., Azzariti, A., Bellizzi, A., and Paradiso, A. (2006) The complexity of targeting EGFR signalling in cancer: from expression to turnover. *Biochim. Biophys. Acta, Rev. Cancer 1766*, 120−139.
(13) Nicholson, R. I., Gee, J. M., and Harper, M. E. (2001) EGFR and cancer prognosis. *Eur. J. Cancer 37*, S9−15.
(14) Miao, Z., Ren, G., Liu, H., Jiang, L., and Cheng, Z. (2010) Cy5.5-labeled affibody molecule for near-infrared fluorescent optical imaging of epidermal growth factor receptor positive tumors. *J. Biomed. Opt. 15*, 036007.
(15) Warram, J. M., de Boer, E., Sorace, A. G., Chung, T. K., Kim, H., Pleijhuis, R. G., van Dam, G. M., and Rosenthal, E. L. (2014) Antibody-based imaging strategies for cancer. *Cancer Metastasis Rev. 33*, 809−822.
(16) Peters, C., and Brown, S. (2015) Antibody−drug conjugates as novel anti-cancer chemotherapeutics. *Biosci. Rep. 35*, e00225.
(17) Diem, M. D., Hyun, L., Yi, F., Hippensteel, R., Kuhar, E., Lowenstein, C., Swift, E. J., O'Neil, K. T., and Jacobs, S. A. (2014) Selection of high-affinity Centyrin FN3 domains from a simple library diversified at a combination of strand and loop positions. *Protein Eng., Des. Sel. 27*, 419−429.
(18) Garland, M., Yim, J.J., and Bogyo, M. A. (2016) Bright future for precision medicine: Advances in fluorescent chemical probe design and their clinical application. *Cell Chemical Biology 23*, 122−136.
(19) Zhang, R. R., Schroeder, A. B., Grudzinski, J. J., Rosenthal, E. L., Warram, J. M., Pinchuk, A. N., Eliceiri, K. W., Kuo, J. S., and Weichert, J. P. (2017) Beyond the margins: real-time detection of cancer using targeted fluorophores. *Nat. Rev. Clin. Oncol. 14*, 347.
(20) Hong, G., Antaris, A. L., and Dai, H. (2017) Near-infrared fluorophores for biomedical imaging. *Nat. Biomed. Eng. 1*, 0010.
(21) Vahrmeijer, A. L., Hutteman, M., van der Vorst, J. R., van de Velde, C. J. H., and Frangioni, J. V. (2013) Image-guided cancer surgery using near-infrared fluorescence. *Nat. Rev. Clin. Oncol. 10*, 507−518.
(22) Okusanya, O. T., Madajewski, B. A., Segal, E., Judy, B. F., Venegas, O. G., Judy, R. P., Quatromoni, J. G., Wang, M. D., Nie, S., and Singhal, S. (2015) Small portable interchangeable imager of fluorescence for fluorescence guided surgery and research. *Technol. Cancer Res. Treat. 14*, 213−220.
(23) Bromme, D., and Wilson, S. (2011) Role of cysteine cathepsins in extracellular proteolysis, In *Extracellular Matrix Degradation* (Parks, W. C., and Mecham, R. P., Eds.) pp 23−51, Springer-Verlag, Berlin Heidelberg.
(24) Mohamed, M. M., and Sloane, B. F. (2006) Cysteine cathepsins: multifunctional enzymes in cancer. *Nat. Rev. Cancer 6*, 764−775.
(25) Powers, J. C., Asgian, J. L., Ekici, O. D., and James, K. E. (2002) Irreversible inhibitors of serine, cysteine, and threonine proteases. *Chem. Rev. 102*, 4639−4650.
(26) Blum, G., Mullins, S. R., Keren, K., Fonovic, M., Jedeszko, C., Rice, M. J., Sloane, B. F., and Bogyo, M. (2005) Dynamic imaging of protease activity with fluorescently quenched activity-based probes. *Nat. Chem. Biol. 1*, 203−209.
(27) Blum, G., von Degenfeld, G., Merchant, M. J., Blau, H. M., and Bogyo, M. (2007) Noninvasive optical imaging of cysteine protease activity using fluorescently quenched activity-based probes. *Nat. Chem. Biol. 3*, 668−677.
(28) Verdoes, M., Oresic Bender, K., Segal, E., van der Linden, W. A., Syed, S., Withana, N. P., Sanman, L. E., and Bogyo, M. (2013) Improved quenched fluorescent probe for imaging of cysteine cathepsin activity. *J. Am. Chem. Soc. 135*, 14726−14730.
(29) Edgington, L. E., Berger, A. B., Blum, G., Albrow, V. E., Paulick, M. G., Lineberry, N., and Bogyo, M. (2009) Noninvasive optical imaging of apoptosis by caspase-targeted activity-based probes. *Nat. Med. 15*, 967−973.
(30) Segal, E., Prestwood, T. R., van der Linden, W. A., Carmi, Y., Bhattacharya, N., Withana, N., Verdoes, M., Habtezion, A., Engleman, E. G., and Bogyo, M. (2015) Detection of intestinal cancer by local, topical application of a quenched fluorescence probe for cysteine cathepsins. *Chem. Biol. 22*, 148−158.
(31) Bender, O. K., Ofori, L., van der Linden, W. A., Mock, E. D., Datta, G. K., Chowdhury, S., Li, H., Segal, E., Sanchez Lopez, M., and Ellman, J. A. (2015) Design of a highly selective quenched activity-based probe and its application in dual color imaging studies of cathepsin S activity localization. *J. Am. Chem. Soc. 137*, 4771−4777.
(32) Verdoes, M., Edgington, L. E., Scheeren, F. A., Leyva, M., Blum, G., Weiskopf, K., Bachmann, M. H., Ellman, J. A., and Bogyo, M. (2012) A nonpeptidic cathepsin S activity-based probe for noninvasive optical imaging of tumorassociated macrophages. *Chem. Biol. 19*, 619−628.
(33) Cutter, J. L., Cohen, N. T., Wang, J., Sloan, A. E., Cohen, A. R., Panneerselvam, A., Schluchter, M., Blum, G., Bogyo, M., and Basilion, J. P. (2012) Topical application of activity-based probes for visualization of brain tumor tissue. *PLoS One 7*, e33060.
(34) Weissleder, R., Tung, C. H., Mahmood, U., and Bogdanov, A., Jr. (1999) In vivo imaging of tumors with protease-activated near-infrared fluorescent probes. *Nat. Biotechnol. 17*, 375−378.
(35) Hu, H. Y., Vats, D., Vizovisek, M., Kramer, L., Germanier, C., Wendt, K. U., Rudin, M., Turk, B., Plettenburg, O., and Schultz, C. (2014) In vivo imaging of mouse tumors by a lipidated cathepsin S substrate. *Angew. Chem., Int. Ed. 53*, 7669−7673.
(36) Ofori, L. O., Withana, N. P., Prestwood, T. R., Verdoes, M., Brady, J. J., Winslow, M. M., Sorger, J., and Bogyo, M. (2015) Design of protease activated optical contrast agents that exploit a latent lysosomotropic effect for use in fluorescence-guided surgery. *ACS Chem. Biol. 10*, 1977−1988.

DOI: 10.1021/acs.bioconjchem.7b00566
Bioconjugate Chem. XXXX, XXX, XXX−XXX

(37) Savariar, E. N., Felsen, C. N., Nashi, N., Jiang, T., Ellies, L. G., Steinbach, P., Tsien, R. Y., and Nguyen, Q. T. (2013) Real-time in vivo molecular detection of primary tumors and metastases with ratiometric activatable cell-penetrating peptides. *Cancer Res. 73*, 855−864.
(38) Ye, D., Shuhendler, A. J., Cui, L., Tong, L., Tee, S. S., Tikhomirov, G., Felsher, D. W., and Rao, J. (2014) Bioorthogonal cyclization-mediated in situ self-assembly of small-molecule probes for imaging caspase activity *in vivo*. *Nat. Chem. 6*, 519−526.
(39) Kanduluru, A., Srinivasarao, M., and Low, P. S. (2016) Design, synthesis, and evaluation of a neurokinin-1 receptor targeted near-IR dye for fluorescence-guided surgery of neuroendocrine cancers. *Bioconjugate Chem. 27*, 2157−2165.
(40) Wayua, C., and Low, P. S. (2014) Evaluation of a cholecystokinin 2 receptor-targeted near-infrared dye for fluorescence-guided surgery of cancer. *Mol. Pharmaceutics 11*, 468−476.
(41) Banerjee, S. R., Pullambhatla, M., Byun, Y., Nimmagadda, S., Foss, C. A., Green, G., Fox, J. J., Lupold, S. E., Mease, R. C., and Pomper, M. G. (2011) Sequential SPECT and optical imaging of experimental models of prostate cancer with a dual modality inhibitor of the prostate-specific membrane antigen. *Angew. Chem., Int. Ed. 50*, 9167−9170.
(42) Chen, Y., Dhara, S., Banerjee, S. R., Byun, Y., Pullambhatla, M., Mease, R. C., and Pomper, M. G. (2009) A low molecular weight PSMA-based fluorescent imaging agent for cancer. *Biochem. Biophys. Res. Commun. 390*, 624−629.
(43) Neuman, B. P., Eifler, J. B., Castanares, M., Chowdhury, W. H., Chen, Y., Mease, R. C., Ma, R., Mukherjee, A., Lupold, S. E., and Pomper, M. G. (2015) Real-time, near-infrared fluorescence imaging with an optimized dye/ light source/camera combination for surgical guidance of prostate cancer. *Clin. Cancer Res. 21*, 771−780.
(44) Guan, G., Lu, Y., Zhu, X., Liu, L., Chen, J., Ma, Q., Zhang, Y., Wen, Y., Yang, L., Liu, T., et al. (2015) CXCR4-targeted near-infrared imaging allows detection of orthotopic and metastatic human osteosarcoma in a mouse model. *Sci. Rep. 5*, 15244.
(45) Lv, P. C., Roy, J., Putt, K. S., and Low, P. S. (2016) Evaluation of a carbonic anhydrase IX-targeted near-infrared dye for fluorescence-guided surgery of hypoxic tumors. *Mol. Pharmaceutics 13*, 1618−1625.
(46) Groves, K., Bao, B., Zhang, J., Handy, E., Kennedy, P., Cuneo, G., Supuran, C. T., Yared, W., Peterson, J. D., and Rajopadhye, M. (2012) Synthesis and evaluation of near-infrared fluorescent sulfonamide derivatives for imaging of hypoxia-induced carbonic anhydrase IX expression in tumors. *Bioorg. Med. Chem. Lett. 22*, 653−657.
(47) Chen, X., Conti, P. S., and Moats, R. A. (2004) In vivo near-infrared fluorescence imaging of integrin $\alpha v\beta 3$ in brain tumor xenografts. *Cancer Res. 64*, 8009−8014.
(48) Choi, H. S., Gibbs, S. L., Lee, J. H., Kim, S. H., Ashitate, Y., Liu, F., Hyun, H., Park, G., Xie, Y., Bae, S., Henary, M., and Frangioni, J. V. (2013) Targeted zwitterionic near-infrared fluorophores for improved optical imaging. *Nat. Biotechnol. 31*, 148−153.
(49) Verbeek, F. P., van der Vorst, J. R., Tummers, Q. R., Boonstra, M. C., de Rooij, K. E., Löwik, C. W., Valentijn, A. R., van de Velde, C. J., Choi, H. S., Frangioni, J. V., et al. (2014) Near-infrared fluorescence imaging of both colorectal cancer and ureters using a low-dose integrin targeted probe. *Ann. Surg Oncol 21*, S528−537.
(50) Boonstra, M. C., van Driel, P. B., van Willigen, D. M., Stammes, M. A., Prevoo, H. A., Tummers, Q. R., Mazar, A. P., Beekman, F. J., Kuppen, P. J., van de Velde, C. J., et al. (2015) uPAR-targeted multimodal tracer for pre- and intraoperative imaging in cancer surgery. *Oncotarget 6*, 14260−14273.
(51) Christensen, A., Juhl, K., Persson, M., Charabi, B. W., Mortensen, J., Kiss, K., Lelkaitis, G., Rubek, N., von Buchwald, C., and Kjær, A. (2017) uPAR-targeted optical near-infrared (NIR) fluorescence imaging and PET for image-guided surgery in head and neck cancer: proof-of-concept in orthotopic xenograft model. *Oncotarget 8*, 15407−15419.
(52) Boonstra, M. C., Tolner, B., Schaafsma, B. E., Boogerd, L. S., Prevoo, H. A., Bhavsar, G., Kuppen, P. J., Sier, C. F., Bonsing, B. A., Frangioni, J. V., et al. (2015) Preclinical evaluation of a novel CEA-targeting near-infrared fluorescent tracer delineating colorectal and pancreatic tumors. *Int. J. Cancer 137*, 1910−1920.
(53) van Driel, P. B., Boonstra, M. C., Prevoo, H. A., van de Giessen, M., Snoeks, T. J., Tummers, Q. R., Keereweer, S., Cordfunke, R. A., Fish, A., van Eendenburg, J. D., et al. (2016) EpCAM as multi-tumour target for near-infrared fluorescence guided surgery. *BMC Cancer 16*, 884.
(54) He, J., Yang, L., Yi, W., Fan, W., Wen, Y., Miao, X., and Xiong, L. (2017) Combination of fluorescence-guided surgery with photodynamic therapy for the treatment of cancer. *Mol. Imaging 16*, 1−15.
(55) Jo, D., and Hyun, H. (2017) Structure-inherent targeting of near-infrared fluorophores for image-guided surgery. *Chonnam Med. J. 53*, 95−102.
(56) Liu, J., Chen, C., Ji, S., Liu, Q., Ding, D., Zhao, D., and Liu, B. (2017) Long wavelength excitable near-infrared fluorescent nanoparticles with aggregation-induced emission characteristics for image-guided tumor resection. *Chem. Sci. 8*, 2782−2789.
(57) Goldberg, S. D., Cardoso, R. M. F., Lin, T., Spinka-Doms, T., Klein, D., Jacobs, S. A., Dudkin, V., Gilliland, G., and O'Neil, K. T. (2016) Engineering a targeted delivery platform using Centyrins. *Protein Eng., Des. Sel.*, 563−572.
(58) Melenhorst, W. B., Mulder, G. M., Xi, Qi, Hoenderop, J. G. J., Kimura, K., Eguchi, S., and van Goor, H. (2008) Epidermal Growth Factor Receptor Signaling in the Kidney. *Hypertension 52*, 987−993.
(59) Natarajan, A., Wagner, B., and Sibilia, M. (2007) The EGF receptor is required for efficient liver regeneration. *Proc. Natl. Acad. Sci. U. S. A. 104*, 17081−17086.
(60) Metastatic Cancer - National Cancer Institute, https://www.cancer.gov/types/metastatic-cancer, February 6, 2017.
(61) Imai, K., and Takaoka, A. (2006) Comparing antibody and small-molecule therapies for cancer. *Nat. Rev. Cancer 6*, 714−727.
(62) Vazquez-Lombardi, R., Phan, T. G., Zimmermann, C., Lowe, D., Jermutus, L., and Christ, D. (2015) Challenges and opportunities for non-antibody scaffold drugs. *Drug Discovery Today 20*, 1271−1283.

DOI: 10.1021/acs.bioconjchem.7b00566
Bioconjugate Chem. XXXX, XXX, XXX−XXX